
POAC'15
Trondheim, Norway

Proceedings of the 23rd International Conference on
Port and Ocean Engineering under Arctic Conditions
June 14-18, 2015
Trondheim, Norway

Observations of Anisotropy in Damage and Elastic Properties of Columnar Ice Containing Cracks

Scott A. Snyder, Erland M. Schulson, Carl E. Renshaw

Ice Research Laboratory, Thayer School of Engineering, Dartmouth College
Hanover, NH 03755 U.S.A.

ABSTRACT

We report a strain-induced anisotropy in elastic properties in columnar ice subjected to uniaxial compressive loading. Polycrystalline specimens of both freshwater ice and saline ice were produced and tested in the laboratory at $-10\,^{\circ}\mathrm{C}$ to explore the effects of damage on mechanical behavior and elastic properties. The tests consisted of 1) imparting inelastic strain by compressing the specimens uniaxially across the columnar grains at constant strain rates, 2) measuring changes in elastic properties (by ultrasonic transmission technique) and microstructure (including damage quantification) and 3) reloading the specimens again in uniaxial compression, either parallel (x_1) or perpendicular (x_2) to the initial loading direction. We observed distinct differences in the character of stress–strain curves recorded upon reloading the specimens in the x_1 versus the x_2 directions. In freshwater ice in particular, this difference coincided with a greater (by 20 percent or more) reduction in the dynamic Young's modulus measured along x_2 compared to x_1. We quantified visible damage by measuring lengths and orientations of crack traces in thin sections cut from the prestrained freshwater ice. For each thin section analyzed, a crack density tensor was computed to compare anisotropy in damage with that measured in the elastic properties.

1 Introduction

Advancements in ice mechanics have built upon, and contributed to, developing understanding of brittle materials in general, including rock, ceramics, and concrete. Such materials, upon deformation, can sustain damage in the form of non-propagating cracks. The length and orientation distributions of these crack systems depend upon the microstructure of the material and on the applied stress. Under uniaxial loading, cracks tend to align parallel to the direction of applied load, although different crack nucleation mechanisms (e.g., dislocation pile-up or grain-boundary sliding) may privilege different orientations (Frost, 2001). A preferential orientation of cracks induces anisotropy in the internal stress fields within the damaged material, and therefore in its effective bulk elastic properties (Kachanov, 1994).

The effects of load-induced anisotropy on elastic properties of rocks and other solids have been copiously studied, for example, using the self-consistent method (Horii and Nemat-Nasser, 1983) and non-interacting crack models (Kachanov, 1982). Others have extended these efforts to more fully describe the coupling of intermediate or meso-scale cracking

and frictional crack sliding (Halm and Dragon, 1998). However, systematic experimental investigations are less common.

Dynamic anisotropy of damage has important implications for the fields of ice engineering and ice rheology. Continuum damage mechanics has shed light on deformation processes in ice (e.g., Jordaan et al., 1992, Xiao and Jordaan, 1996), albeit under the assumption that damage is isotropic. Under certain flow conditions, the velocity of ice sheets can be highly dependent on the degree of anisotropy of damage contained in the ice (Pralong et al., 2006). Early studies of cracking activity in ice during creep reported a preference for cracks to form in planes close to parallel to the direction of applied load (Gold, 1960), and to form in or adjacent to grains oriented unfavorably for plastic slip, in columnar ice (Gold, 1972) and in granular ice (Cole, 1986). Strain-induced viscoplastic anisotropy in ice has been well-characterized, resulting from the very low resistance to glide along the basal plane in ice (Ih) compared to its other crystal directions (Duval et al., 1983). Statistics regarding crack positions and their spatial density in columnar ice after low levels of strain ($\varepsilon < 0.001$) were reported by Gold (1997, 1999). In granular ice, anisotropic fracture patterns were studied by Weiss and Gay (1998), but few reports can be found that link experimental quantification of damage to the mechanical properties of ice.

In preliminary tests to study damage effects in columnar ice (Snyder et al., 2013), we found unexpected evidence of anisotropy in the stress–strain curves recorded during subsequent reloading of prestrained ice, at $-10\,^{\circ}\mathrm{C}$. Figure 1 shows representative curves for freshwater ice specimens that had been uniaxially prestrained to $\varepsilon_{\mathrm{p}} = 0.035$ compression at constant strain rate $\dot{\varepsilon}_{\mathrm{p}} = 1 \times 10^{-5}\,\mathrm{s}^{-1}$. Upon reloading (again in uniaxial compression) at a rate below the ductile-to-brittle transition and in the x_1 direction, *parallel* to initial loading, a characteristic stress peak occurred that increased with strain rate (Fig. 1 top row). When reloading was instead in x_2, *perpendicular* to initial loading, the stress did not exhibit a peak (Fig. 1 bottom row). Instead, the stress increased in a usual way until about 1 MPa, at which point there was a clear shift in the apparent modulus and stress continued to rise with increasing strain along a lower positive slope, until the tests were ended after additional strain of 0.03.

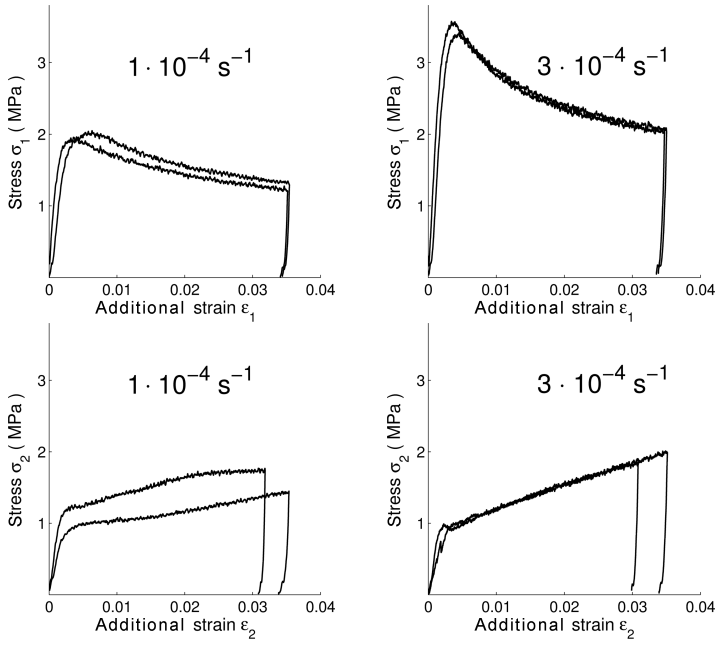

Figure 1: Stress–strain curves during uniaxial compressive reloading of freshwater ice that had been prestrained to $\varepsilon_{\mathrm{p}} = 0.035$ at $1 \times 10^{-5}\,\mathrm{s}^{-1}$ in x_1. Reloading was in x_1 (top row) or in x_2 (bottom row) at the strain rate indicated on the graphs. Two tests are plotted at each condition to show that the general shape of the curves was reproducible despite minor variations between subspecimens.

We do not yet have a good explanation for this anisotropy in the mechanical response of damaged ice under compressive load. The goal of this paper is to disseminate our observations pertaining to other anisotropic aspects of damaged ice, namely crack density and Young's modulus, in order to motivate further research that could provide better understanding of these phenomena.

2 Experimental procedure

Ice was grown and prepared in the laboratory for use in these experiments. The test procedure consisted of 1) imparting inelastic strain by compressing the specimens uniaxially across the columnar grains at constant strain rates, 2) measuring changes in elastic properties (by ultrasonic transmission technique) and microstructure (including damage quantification) and 3) reloading the specimens again in uniaxial compression, either parallel (x_1) or perpendicular (x_2) to the initial loading direction. Both freshwater and saline columnar ice, simulating that which is found in nature, was produced following a standard procedure that, along with steps 1) and 2), is described in detail elsewhere (Snyder et al., 2015). An important feature of the ice was that it possessed an S2 texture, in which the c-axes of columnar crystal grains are randomly oriented within but confined to (within about 15°) the horizontal plane relative to the vertical growth direction of the ice. Thus the ice began with elastic orthotropy, facilitating detection of any damage-induced anisotropy.

In step 3), subspecimens sectioned from the prestrained parent specimen, as illustrated in Figure 2, were individually reloaded uniaxially at a strain rate ranging from $1 \times 10^{-6}\,\mathrm{s}^{-1}$ to $3 \times 10^{-2}\,\mathrm{s}^{-1}$. Elapsed time between steps 1) and 3) was (24 ± 4) h. All tests were conducted at $-10\,^{\circ}\mathrm{C}$. Full analysis of the results of step 3) will be published in a forthcoming report.

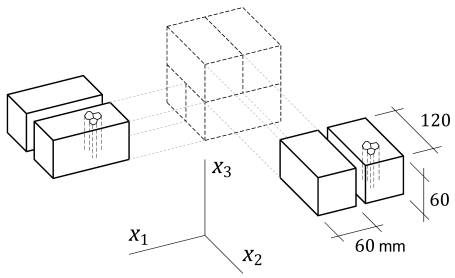

Figure 2: Typical specimen geometry. The cube-shaped parent specimen, after being prestrained under uniaxial across-column compression along x_1, yielded two pairs of subspecimens oriented lengthwise in either the x_1 or x_2 direction.

Damage was quantified by measuring individual crack traces in the thin sections photographed under scattered light. Specifically, we measured the half-length c and the angle θ, from the horizontal axis $(x_2)^*$, of each crack trace in the plane of the thin section, as shown in Figure 3.

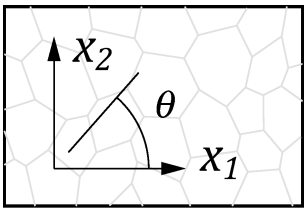

Figure 3: Coordinate system x_1–x_2 in the plane perpendicular to columnar grains. Ice specimens were prestrained in the x_1 direction. The angle θ measures the inclination of crack traces within across-column thin sections.

*In this paper, we will consider measurements made from across-column (x_1–x_2) thin-section orientations only. See Snyder et al. (2015) for an account of the complications involved in measuring crack densities from along-column thin sections, due to the attenuated geometry of the grains.

We used the two-dimensional crack density tensor (Kachanov, 1994)

$$\alpha = \frac{1}{A}\sum_i (c^2 nn)_i \tag{1}$$

where n is a unit vector normal to the ith crack trace. In the summation, nn denotes the dyadic, or outer product. n has components $(n_1,\ n_2) = (-\sin\theta,\ \cos\theta)$. As a symmetric second-rank tensor, α can be transformed into its principal coordinate representation with eigenvalues $\alpha_{1'}$ and $\alpha_{2'}$ as the only non-zero components.

3 Results

The thin sections shown in Figure 4 demonstrate visually how damage increased with prestrain. Figure 5 plots the half-length c versus inclination angle θ of crack traces measured in across-column thin sections. N denotes the average number of cracks traced in each thin section for each prestrain condition. Note that N for $\dot{\varepsilon}_p = 1 \times 10^{-6}\,s^{-1}$ is about two-thirds

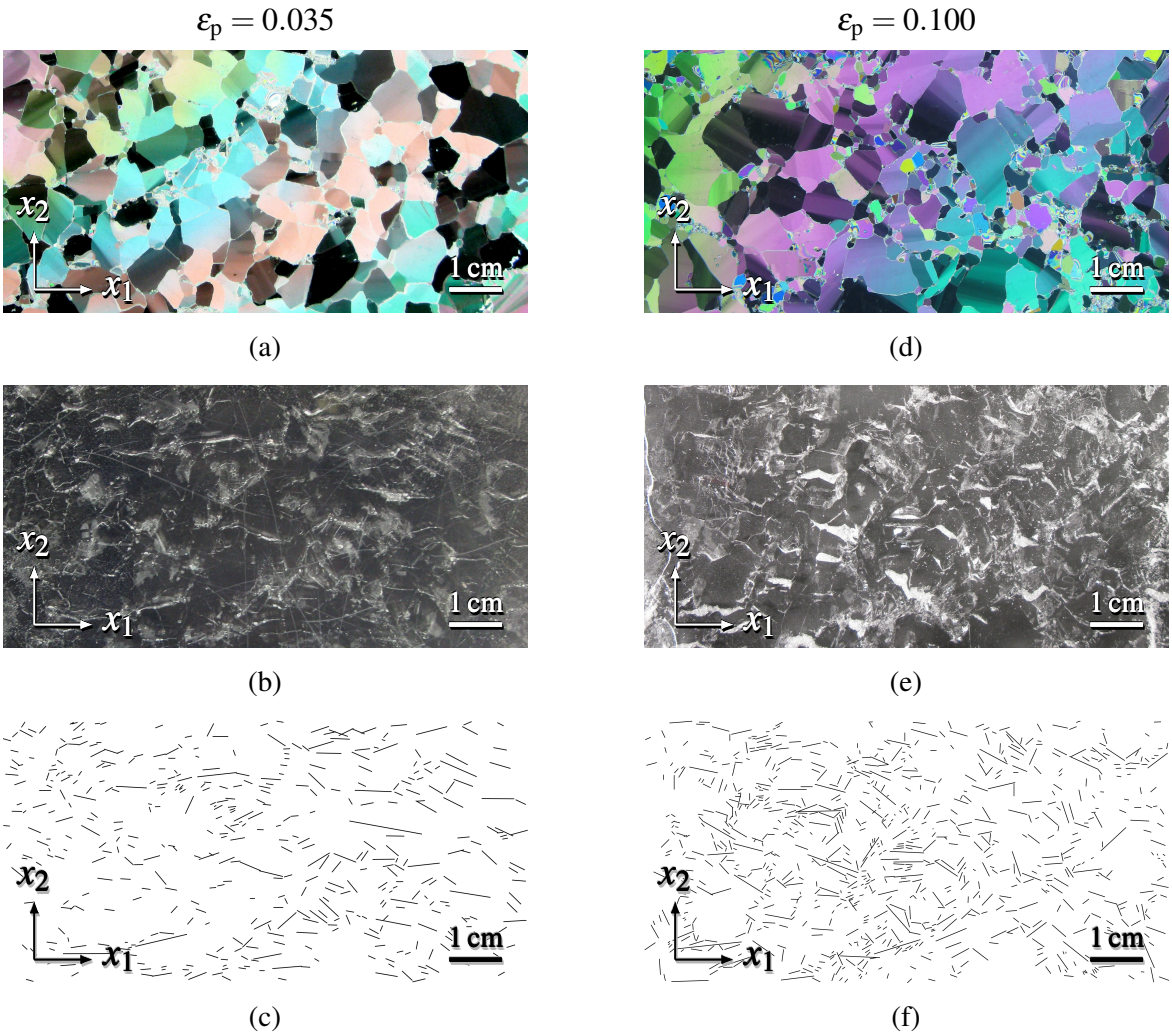

Figure 4: Thin sections of columnar-grained freshwater ice after prestrain (left column) $\varepsilon_p = 0.035$ and (right column) $\varepsilon_p = 0.100$ at $1 \times 10^{-5}\,s^{-1}$ at $-10\,°C$. Crossed-polarized light revealed the grain structure in (a) and (d). The cracks seen under scattered light in (b) and (e) were digitally traced to produce the fracture patterns shown in (c) and (f).

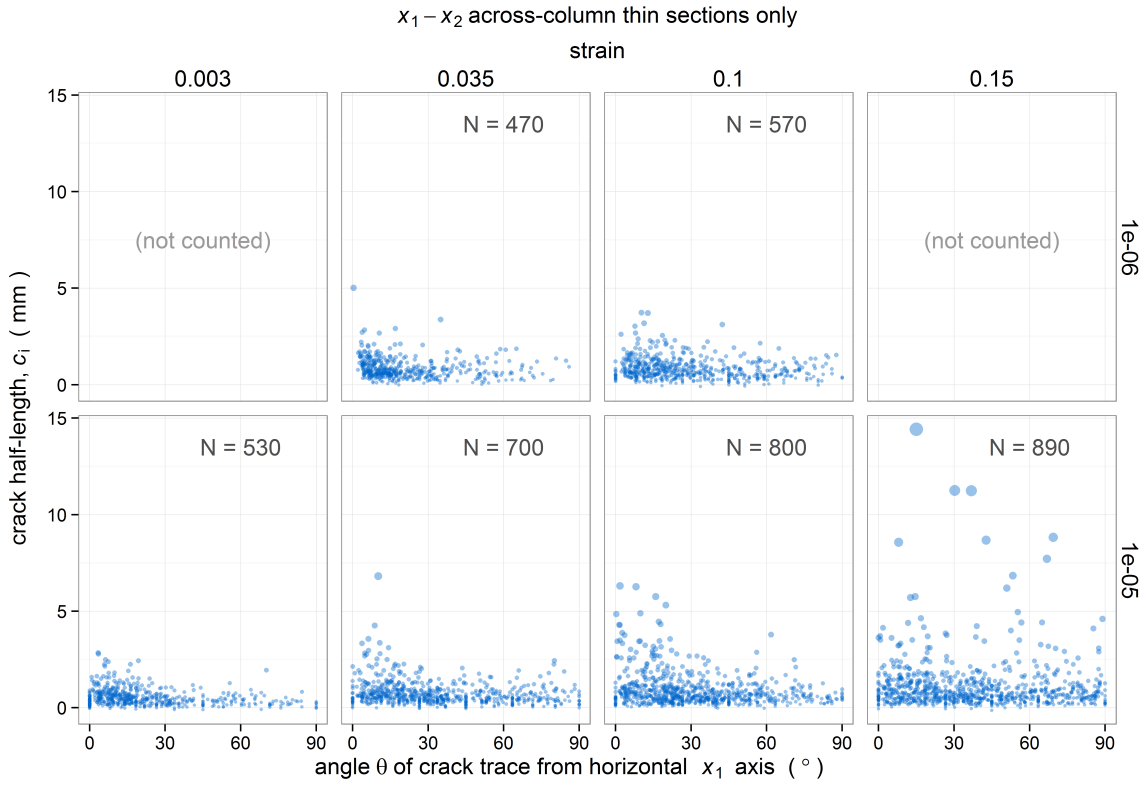

Figure 5: Distribution of sizes and angles of crack traces in across-column thin sections of prestrained freshwater ice. The level of prestrain increases from left to right as indicated above the panels, imparted at $1 \times 10^{-6}\,\mathrm{s}^{-1}$ (top row) or $1 \times 10^{-5}\,\mathrm{s}^{-1}$ (bottom row). Each panel plots the half-length c versus inclination angle θ for a random sampling of N crack trace measurements, where N is the mean number of cracks counted in a $50\,\mathrm{cm}^2$ thin-section area for each condition.

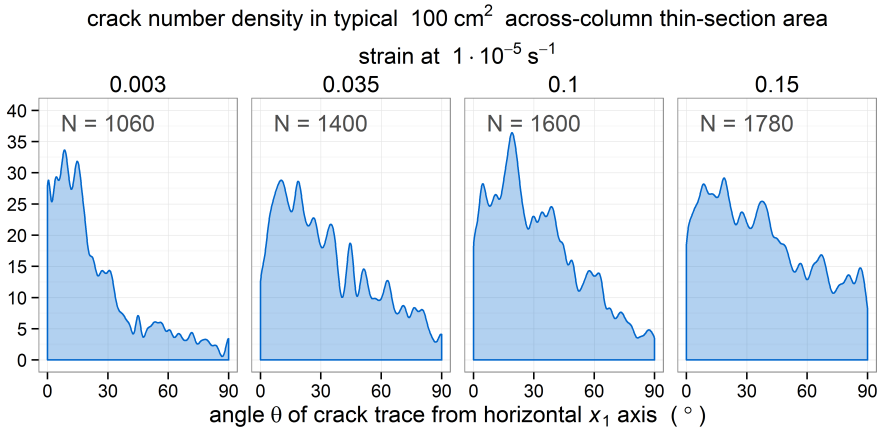

Figure 6: Distribution of inclination angle θ of cracks traced in across-column thin sections of freshwater ice, after various levels of prestrain imparted in the x_1 direction at $1 \times 10^{-5}\,\mathrm{s}^{-1}$. Each panel plots the probability density function (scaled by the number of observations) for a random sampling of N crack trace measurements.

the number for $\dot{\varepsilon}_p = 1 \times 10^{-5}\,s^{-1}$, for the two levels of prestrain ($\varepsilon_p = 0.035$ and $\varepsilon_p = 0.10$) tested at both rates. At every condition tested, the majority of cracks were shorter than the mean grain diameter of (5 ± 2) mm. As prestrain increased, cracks at greater lengths were seen in greater quantities. Up to $\varepsilon_p = 0.10$, the longer crack traces followed a similar orientation distribution as the population, with the peak inclinations within 10° to 20° of the x_1 axis, even as the population distribution began to even out.

Focusing on the orientation statistics, Figure 6 plots the number density (i.e., probability density function scaled by the number of observations) of crack traces measured in a typical across-column thin-section area of 100 cm^2. The distribution of crack angles is positively skewed at $\varepsilon_p = 0.003$ (resembling the distribution observed by Gold (1960) in cracks formed in ice under constant stress of about 1.4 MPa) and becomes more uniform at higher levels of prestrain. This suggests that, beyond initial damage, further prestrain suppresses anisotropy in crack orientation distribution.

The unit normal vector n and half-length c of each crack trace were entered into the summation of Equation 1 to determine the four components of the crack density tensor α. The non-zero principal coordinate components (eigenvalues) $\alpha_{1'}$ and $\alpha_{2'}$ were found to differ from α_{11} and α_{22}, in specimen coordinates, by no more than 3 % and 6 %, respectively. In other words, the principal directions of α were closely aligned to the specimen coordinates x_1 and x_2, reflecting the preferential orientation of cracks.

Figure 7 plots the ratio of crack density tensor components, α_{22}/α_{11}, in specimen coordinates, as a function of prestrain ε_p. The crack density components in undamaged ice, of course, were zero; the ratio there (at $\varepsilon_p = 0$) is plotted as unity for reference. The trend shows a near linear decrease in α_{22}/α_{11}, regardless of prestrain rate. This result is consistent with

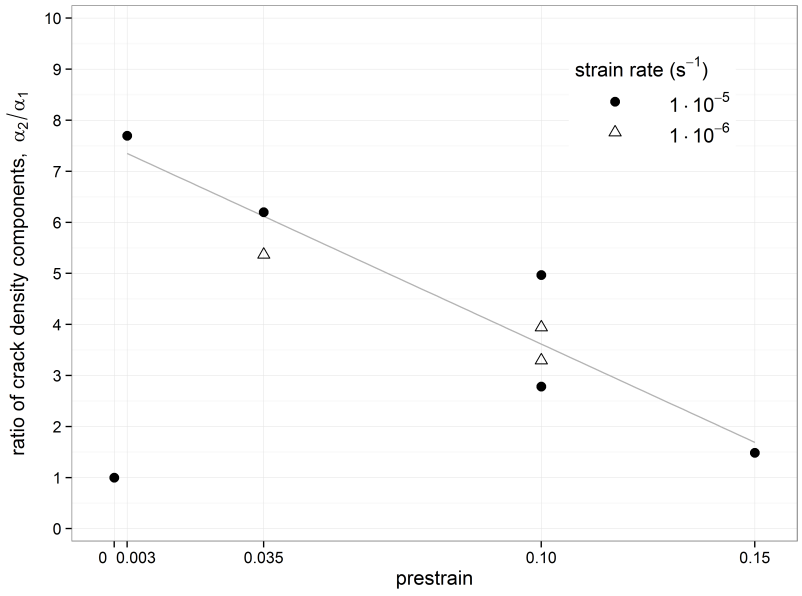

Figure 7: Ratio of dimensionless crack density tensor components, α_{22}/α_{11} as a function of compressive prestrain in freshwater ice applied uniaxially in the x_1 direction at the strain rate indicated in the legend. Crack density was determined by tracing cracks in thin sections cut across the columnar grains, through the center of the prestrained ice specimens. The crack density components are based on vectors normal to each crack trace, so that a ratio α_{22}/α_{11} greater than unity indicates a dominance of crack orientations parallel to the x_1 direction.

how the distribution of crack orientations was seen to evolve (Fig. 5). It is also in agreement with previous reports of fracture patterns in granular ice, in which anisotropy decreased with increasing strain (Weiss and Gay, 1998).

Consider the crack orientation distribution density $\rho(\theta)$ for $\varepsilon_p = 0.003$. The ratio of the peak distribution to the average, $\rho_{max}/\langle\rho\rangle$, is about 3. Such a ratio represents a noticeably non-isotropic damage distribution that, according to the non-interacting crack model of damage in 2–D (Kachanov, 1994), should result in elastic anisotropy in which $E_2/E_1 \approx 0.85$. Under that model, for the same level of damage, ideally parallel cracks give $E_2/E_1 = 0.76$, while for isotropic damage, of course, $E_2/E_1 = 1$.[†] Let us see how our elastic moduli data compare.

Figure 8 is a graph of elastic anisotropy parameter ζ as a function of prestrain. We define this anisotropy parameter as

$$\zeta \triangleq (E_1 - E_2)/E_1 = 1 - (E_2/E_1) \tag{2}$$

based on the ratio of dynamic Young's moduli. The E_1 and E_2 data used to calculate the plotted ratios represent the average of three or more readings of ultrasonic transmission velocities made on each of two right-prismatic subspecimens, which had their long dimensions (the direction of acoustic wave propagation) parallel to x_1 or x_2, respectively (Fig. 2). In the graph, solid blue lines (freshwater ice) and broken green lines (saline ice) connect the mean values of ζ in each group from the lower strain rates in both types of ice. Positive values of ζ attest to greater stiffness in the x_1 direction compared to x_2; negative values, the reverse.

[†]Note that our x_1–x_2 coordinates are reversed from the system used by Kachanov, who considered stress to be applied in the x_2 direction.

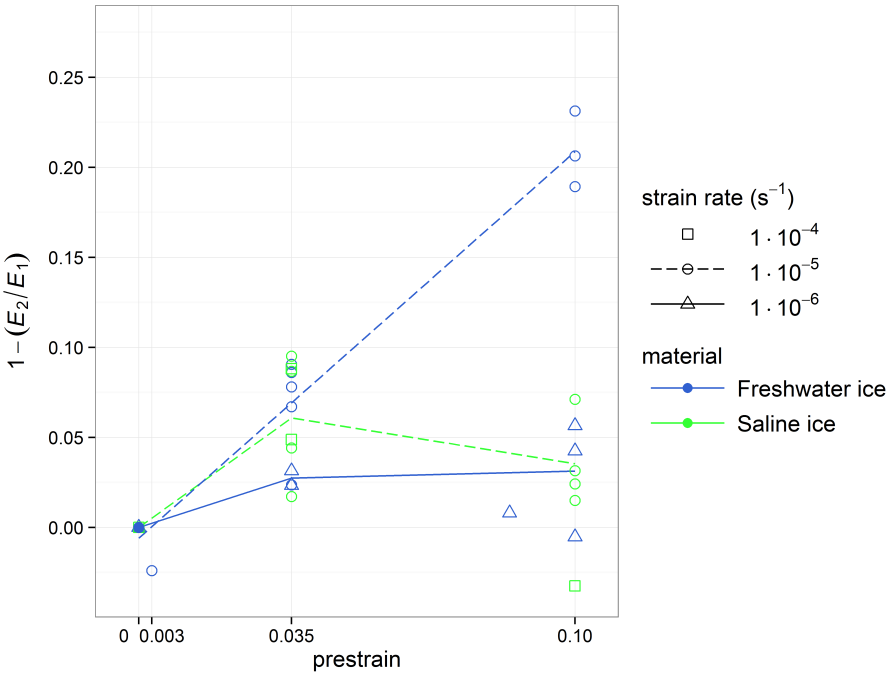

Figure 8: Anisotropy parameter, $1 - (E_2/E_1)$, as a function of prestrain. E_1 and E_2 are the dynamic Young's moduli measured in the x_2 and x_1 directions, respectively. For both freshwater and saline ice, compressive prestrain was applied uniaxially in the x_1 direction, at the strain rate indicated in the legend.

A small but detectable positive elastic anisotropy is seen in both types of ice at $\varepsilon_p = 0.035$. At that level of prestrain, the anisotropy shows a minor dependence on strain rate in freshwater ice, with ζ increasing from about 0.025 at the lower strain rate to 0.070 at the higher strain rate. This observation may seem somewhat questionable given the high scatter in the saline ice data, with values for ζ ranging from 0.020 to 0.095 there. However, saline ice exhibited greater variation in general, not only in elastic properties but in mass density as well, whether undamaged or prestrained. The average sample standard deviation in Young's modulus was 0.6 GPa in saline ice, twice what it was in freshwater ice (Snyder et al., 2015).

A significant strain rate effect appears at $\varepsilon_p = 0.10$ in the case of freshwater ice. In contrast, given the uncertainty in accuracy, the ratio E_2/E_1 remained essentially unchanged with respect to prestrain, for saline ice and for freshwater ice prestrained at $1 \times 10^{-6}\,\mathrm{s}^{-1}$. In the case of freshwater ice prestrained at $1 \times 10^{-5}\,\mathrm{s}^{-1}$, the ratio E_2/E_1 departed much farther from unity. This case was fitted by a least squares linear regression, shown by the broken blue line with a slope of 2.1.

The regression includes the odd data point at $\varepsilon_p = 0.003$, which showed negative anisotropy ($\zeta \approx -0.025$). At this low level of strain, we observed—as other investigators have witnessed previously (Weiss and Schulson, 2000)—relatively few transgranular microcracks compared to a prevalence of decohesions along grain-boundaries. These decohesions were not easily distinguished from intergranular cracks, but both kinds of features tended to be longer (in x_3) than the wavelength corresponding to the resonant frequency of the ultrasonic transducers used to make the elastic measurements. Many of these long features appeared as much shorter crack traces in transversely cut x_1–x_2 thin sections. Such traces at $\varepsilon_p = 0.003$ were seen to strongly prefer orientations within 20° of parallel to the x_1 direction (Fig. 6). In other words, our E_1 measurements may be biased higher than the 'true' values, despite the preponderance of these fracture features which could have contributed to high anisotropy in crack density components (Fig. 7). At the least, we know that damage was three-dimensional and therefore unable to be fully quantified by the two-dimensional traces to which our analysis was restricted.

It is worth recalling that the crack density tensor α was developed in the context of a damage model based on Mode–I stress fields around cracks (although the model can be extended to incorporate Mode–II and Mode–III stress concentrations produced by crack sliding under compression; see Kachanov, 1994). Under compressive stress states, the process of crack closure itself leads to elastic anisotropy (Horii and Nemat-Nasser, 1983). We attempted—but were unsuccessful—to detect a change in Young's modulus by making ultrasonic readings while the specimen was held under various loads from 1 kN, 2 kN, 3 kN and 4 kN. As increasing loads were applied to those specimens, however, we observed the nucleation of additional cracks, which may have obscured any increase in stiffness that could otherwise have resulted from closure of the pre-existing cracks. The possible influence of crack closure and frictional sliding both require further investigation.

Regarding saline ice prestrained at the higher rate, $\dot{\varepsilon}_p = 1 \times 10^{-4}\,\mathrm{s}^{-1}$ (Fig. 8, green squares), it is possible there is a significant but opposite effect of ε_p on ζ being demonstrated in those data, too. Compare $\zeta \approx 0.05$ (at $\varepsilon_p = 0.035$) to $\zeta \approx -0.03$ (at $\varepsilon_p = 0.10$). The data are too few to draw definitive conclusions.

The reason for the selective strain rate dependence in ζ in freshwater ice is not yet understood. If cracks were the only factor reducing effective stiffness, one would expect the anisotropy in damage to follow a similar pattern as ζ, but the crack density data refute this correspondence. The disparity between freshwater ice and saline ice could be partly

attributable to a material difference. Saline ice is initially a more porous material, so the nature of damage may differ between freshwater and saline ice.[‡] A cautionary remark: we should not assign undue importance to the interpolation suggested by the linear fit (Fig. 8). There may be a discontinuity that occurs near strains of 0.10; indeed, it is at this level of prestrain and greater that we began to see a change in the nature of damage, with cracks opening widely—from a few millimeters at $\varepsilon_p = 0.10$ (Fig. 4e) up to tens of millimeters wide at $\varepsilon_p > 0.10$. In addition, we must remain aware that processes unrelated to cracking (e.g., recrystallization) were also occurring as the specimens were strained in the ductile regime. The anisotropy in evidence here is likely the result of multiple factors interacting, and more work is needed to draw those factors apart.

4 Summary

We summarized experiments on freshwater and saline ice that studied the effects of prestrain on elastic properties. The results revealed anisotropy in crack density and in elastic moduli, although the two were not directly in correspondence. In particular, freshwater ice exhibited an elastic anisotropy that appeared strongly dependent on prestrain and on prestrain rate (Fig. 8). For freshwater ice specimens prestrained to $\varepsilon_p = 0.10$ at $\dot{\varepsilon}_p = 1 \times 10^{-5}\,\mathrm{s}^{-1}$, the elastic anisotropy parameter ($\zeta = (E_1 - E_2)/E_1$) reached above 0.20. In contrast, ζ averaged about 0.03 in other specimens tested at that level: saline ice at the same strain rate, and freshwater ice at a strain rate one order of magnitude lower.

Anisotropy in crack density, on the other hand, appeared the most extreme at low levels of damage and consistently diminished with increasing prestrain regardless of prestrain rate. A tensorial quantification of damage, computed from two-dimensional analysis of thin sections, allowed us to compare anisotropy in terms of crack density at various levels of prestrain. When measured in across-column x_1–x_2 directions, the ratio of crack density components, α_{22}/α_{11}, decreased with increasing prestrain in a near linear fashion, by about a factor of two from $\varepsilon_p = 0.003$ to $\varepsilon_p = 0.10$ (Fig. 7).

These observations provide insight into the non-uniform evolution of damage in columnar ice. More research is warranted to understand the broader scope of implications of this strain-induced anisotropy.

5 Acknowledgements

This work was supported by the U.S. Department of the Interior–Bureau of Safety and Environmental Enforcement (BSEE), contract no. E12PC00033. The authors thank the reviewers for their constructive comments.

References

Cole, D. M. (1986), Effect of grain size on the internal fracturing of polycrystalline ice, CRREL Report 86-5, U.S. Army Cold Regions Research and Engineering Laboratory, Hanover, New Hampshire.

Duval, P., Ashby, M. F. and Anderman, I. (1983), 'Rate-controlling processes in the creep of polycrystalline ice', *The Journal of Physical Chemistry* **87**(21), 4066–4074.

Frost, H. (2001), 'Mechanisms of crack nucleation in ice', *Engineering Fracture Mechanics* **68**(1718), 1823–1837.

[‡]We were unable to unambiguously quantify damage in saline ice due to the presence of pores and brine features (Snyder et al., 2015).

Gold, L. W. (1960), 'The cracking activity in ice during creep', *Canadian Journal of Physics* **38**(9), 1137–1148.

Gold, L. W. (1972), 'The process of failure of columnar-grained ice', *Philosophical Magazine* **26**(2), 311–328.

Gold, L. W. (1997), 'Statistical characteristics for the type and length of deformation-induced cracks in columnar-grain ice', *Journal of Glaciology* **43**(144), 311–320.

Gold, L. W. (1999), 'Statistical characteristics for the strain-dependent density and the spatial position for deformation-induced cracks in columnar-grain ice', *Journal of Glaciology* **45**(150), 264–272.

Halm, D. and Dragon, A. (1998), 'An anisotropic model of damage and frictional sliding for brittle materials', *European Journal of Mechanics - A/Solids* **17**(3), 439–460.

Horii, H. and Nemat-Nasser, S. (1983), 'Overall moduli of solids with microcracks: Load-induced anisotropy', *Journal of the Mechanics and Physics of Solids* **31**(2), 155–171.

Jordaan, I. J., Stone, B. M., McKenna, R. F. and Fuglem, M. K. (1992), 'Effect of microcracking on the deformation of ice', *Canadian Geotechnical Journal* **29**(1), 143–150.

Kachanov, M. L. (1982), 'A microcrack model of rock inelasticity Part I: Frictional sliding on microcracks', *Mechanics of Materials* **1**(1), 19–27.

Kachanov, M. L. (1994), Elastic solids with many cracks and related problems, *in* J. W. Hutchinson and T. Y. Wu, eds, 'Advances in Applied Mechanics', Vol. 30, Academic Press, pp. 259–445.

Pralong, A., Hutter, K. and Funk, M. (2006), 'Anisotropic damage mechanics for viscoelastic ice', *Continuum Mechanics and Thermodynamics* **17**(5), 387–408.

Snyder, S. A., Schulson, E. M. and Renshaw, C. E. (2013), Effects of pre-strain on the elastic properties and the ductile-to-brittle transition of columnar ice, *in* 'POAC'13 Proceedings of the 22nd International Conference on Port and Ocean Engineering under Arctic Conditions'.

Snyder, S. A., Schulson, E. M. and Renshaw, C. E. (2015), 'The role of damage and recrystallization in the elastic properties of columnar ice', *Journal of Glaciology* (In press).

Weiss, J. and Gay, M. (1998), 'Fracturing of ice under compression creep as revealed by multifractal analysis', *Journal of Geophysical Research* **103**(B10), 24005–24016.

Weiss, J. and Schulson, E. M. (2000), 'Grain-boundary sliding and crack nucleation in ice', *Philosophical Magazine A* **80**(2), 279–300.

Xiao, J. and Jordaan, I. J. (1996), 'Application of damage mechanics to ice failure in compression', *Cold Regions Science and Technology* **24**(3), 305–322.